Targeted Deletion of *Rad9* in Mouse Skin Keratinocytes Enhances Genotoxin-Induced Tumor Development

Zhishang Hu,[1,2] Yuheng Liu,[1,2] Chunbo Zhang,[3] Yun Zhao,[1,2] Wei He,[1,2] Lu Han,[1,2] Leilei Yang,[4] Kevin M. Hopkins,[5] Xiao Yang,[4] Howard B. Lieberman,[5,6] and Haiying Hang[1,2]

[1]National Laboratory of Biomacromolecules, and [2]Center for Infection and Immunity, Institute of Biophysics, Chinese Academy of Sciences, [3]College of Life Science, Capital Normal University, and [4]Genetic Laboratory of Development and Diseases, Institute of Biotechnology, Beijing, China; and [5]Center for Radiological Research, College of Physicians and Surgeons and [6]Department of Environmental Health Sciences, Columbia University, Mailman School of Public Health, New York, New York

Abstract

The *Rad9* gene is evolutionarily conserved from yeast to humans and plays crucial roles in genomic maintenance, DNA repair, and cell cycle checkpoint controls. However, the function of this gene with respect to tumorigenesis is not well-understood. A *Rad9*-null mutation in mice causes embryonic lethality. In this study, we created mice in which mouse *Rad9, Mrad9*, was deleted only in keratinocytes to permit examination of the potential function of the gene in tumor development. Mice with $Mrad9^{+/-}$ or $Mrad9^{-/-}$ keratinocytes showed no overt, spontaneous morphologic defects and seemed similar to wild-type controls. Painting the carcinogen 7,12-dimethylbenzanthracene (DMBA) onto the skin of the animals caused earlier onset and more frequent formation of tumors and senile skin plaques in $Mrad9^{-/-}$ mice, compared with $Mrad9^{+/-}$ and $Mrad9^{+/+}$ littermates. DNA damage response genes *p21, p53*, and *Mrad9B* were expressed at higher levels in $Mrad9^{-/-}$ relative to $Mrad9^{+/+}$ skin. Keratinocytes isolated from $Mrad9^{-/-}$ skin had more spontaneous and DMBA-induced DNA double strand breaks than $Mrad9^{+/+}$ keratinocytes, and the levels were reduced by incubation with the antioxidant epigallocatechin gallate. These data suggest that *Mrad9* plays an important role in maintaining genomic stability and preventing tumor development in keratinocytes. [Cancer Res 2008;68(14):5552–61]

Introduction

Cells are constantly exposed to endogenous and exogenous conditions that cause stresses and can induce genomic DNA lesions. Eukaryotic cells have evolutionarily conserved mechanisms that monitor and coordinate cell cycle progression, through checkpoint control activities, with repair of DNA damage. Mutations in genes that play roles in cell cycle checkpoint control and DNA repair are often associated with tumorigenesis. For example, targeted deletion of *p53, Brca1*, or *Atm* cell cycle checkpoint genes enhances tumor development (1–5). *Rad9* plays important roles in multiple cell cycle checkpoint controls and DNA repair (6–8). Hence, *Rad9* is likely a gatekeeper gene that prevents cancer development by promoting repair of DNA damage before deleterious effects ensue.

Several recent studies showed that *Rad9* was aberrantly expressed in tumors. High expression was detected in human non–small cell lung carcinomas (9) and breast tumors (10). A significantly higher frequency of a single nucleotide polymorphism was observed at the second position of codon 239 (*His/Arg* heterozygous variant) in human non–small cell lung carcinomas (11). In contrast, *Rad9* expression levels were found to be lower in prostate cancers in an analysis of three pairs of prostate normal/cancer tissue (12) but a much more extensive analysis found the opposite to be true (13). In fact, aberrantly high levels of Rad9 have been functionally linked to prostate cancer. Combined haploinsufficiency for mouse *atm* and *Mrad9* causes sensitivity to the morphologic transformation of mouse embryonic fibroblasts by ionizing radiation, whereas haploinsufficiency of *Mrad9* alone does not confer a predisposition to transformation (14). The aforementioned studies established a correlation between cancer development and abnormal *Rad9* expression or polymorphism. With respect to expression, aberrantly high or low levels of the protein can predispose to carcinogenesis. However, it remains unclear whether this effect on cancer development is significant for other cancer types, or what the underlying molecular mechanism might be.

A homozygous *Rad9*-null mutation causes mouse embryonic lethality (15); thus, this animal model cannot be used to test whether *Rad9* deletion influences tumorigenesis. In this study, we constructed mice selectively deleted for *Mrad9* in keratinocytes, thereby circumventing issues related to animal viability. Mice with $Mrad9^{+/-}$ or $Mrad9^{-/-}$ keratinocytes showed no overt, spontaneous, morphologic defects. However, the application of 7,12-dimethylbenzanthracene (DMBA) to skin induced a dramatically higher rate of tumor formation in $Mrad9^{-/-}$ mice than in $Mrad9^{+/+}$ or $Mrad9^{+/-}$ controls. Isolated $Mrad9^{-/-}$ keratinocytes showed enhanced DNA lesions compared with $Mrad9^{+/+}$ or $Mrad9^{+/-}$ keratinocytes. The $Mrad9^{-/-}$ cells had aberrant cell cycle distribution and an increased rate of apoptosis. These data suggest that *Mrad9* is critical for maintaining genomic stability and preventing tumor development.

Materials and Methods

Mouse strains and genotyping. To create skin-conditional *Mrad9* knockout mice, $Mrad9^{Tar/Tar}$ (15) 129SvEv strain animals were mated to *Keratin 5-Cre* transgenic mice in which *Cre* expression is under the control of the *Keratin 5* promoter specifically activated in keratinocytes (16). *Keratin 5-Cre* transgenic mice were originally created using Chinese KM mice and then mated with C57BL/6 mice at least for 10 generations, so it is a hybrid of KM and C57BL/6 mice but with more C57BL/6 genetic

Requests for reprints: Haiying Hang, Institute of Biophysics, Chinese Academy of Sciences, 15 Datun Road, Chaoyang District, Beijing 100101, China. Phone/Fax: 86-010-6488-8473; E-mail: hh91@sun5.ibp.ac.cn or Xiao Yang, Genetic Laboratory of Development and Diseases, Institute of Biotechnology, 20 Dongdajie, Beijing 100071, China. Phone/Fax: 86-10-63895937; E-mail: yangx@nic.bmi.ac.cn or Howard B. Lieberman, Center for Radiological Research, Columbia University, 630 West 168th St., New York, NY 10032. Phone: 212-305-9241; Fax: 212-342-5505; E-mail: lieberman@cancercenter.columbia.edu.

doi:10.1158/0008-5472.CAN-07-5670

background. Methods for DNA isolation and PCR genotyping of mouse tissues as well as isolated keratinocytes for the *Mrad9-loxP* loci and *Cre*-mediated recombination were similar to procedures described (15). To detect the presence of the targeted sequence, primers 5′-TTCGGGTGGGAGAATCAGAC-3′ (T1) and 5′-GGATCTCTCCCCATTCACCA-3′ (T2) were used (Fig. 1*A*). To detect the first two exons of *Mrad9*, primers 5′-CCGGGTGAACCAATAAGGAA-3′ (D1) and 5′-AAGGAAGCAGGCATAGGCAG-3′ (D2) were used. PCR conditions were 95°C for 5 min to initially denature DNA, then 35 cycles at 95°C for 30 s, 55°C for 1 min, 72°C for 1 min, and a final extension at 72°C for 5 min. The final reaction mix (25 μL) contained 1× Easy Taq SuperMix (TransGen Biotech Co), 1 μL genomic DNA, and 10 pmol of each primer. All of the animal handling for these protocols and in the following procedures was performed following methods approved by the Institutional Animal Care and Use Committee at the Institute of Biophysics, Chinese Academy of Sciences.

Semiquantitative genomic PCR. To examine *Mrad9*-deletion efficiency in mouse keratinocytes, one sequence downstream of the targeted site was used as template for a DNA loading control. The DNA fragment was generated by PCR using primers 5′-TTCTGTCCTTTCCCCTTGCA-3′ and 5′-GGAGGAAAGCAACAAGTCCT-3′. PCR conditions were the same as described above for genotyping except 60°C was used as the annealing temperature and 28 cycles were run. Genotyping for the successful targeting and deletion of *Mrad9* was carried out with the same method described above.

Reverse transcription-PCR. Total RNA was prepared from epidermis of newborn mice using the RNeasy Mini kit (QIAGEN), as described by the manufacturer. For reverse transcription-PCR (RT-PCR), 2 μg total RNA were reverse transcribed in a 20 μL reaction volume to form cDNA using the SuperScript First-Strand Synthesis System for RT-PCR (Invitrogen). PCR amplification of *Mrad9* was performed using 1 μL of the cDNA generated above and the primer pair: 5′-CTCTATCTGGAACCCTTGAAGGACG-3′ and 5′-CGCAATAAGTGAGGGCATGAGG-3′. Results were normalized to the amount of a PCR-amplified *GAPDH* fragment using 1 μL of cDNA and primers 5′-GCAAAGTGGAGATTGTTGCC-3′ and 5′-CCGTATTCATTGTCATACCA-3′. For *Mrad9* PCR amplification, there was an initial DNA template denaturation at 95°C for 3 min, then 30 cycles of 95°C for 30 s, 60°C for 1 min, 72°C for 30 s, and a final extension at 72°C for 3 min. *GAPDH* PCR conditions were the same as for *Mrad9* except the procedure lasted only 20 cycles.

Quantitative real-time RT-PCR. Total RNA and cDNA from mouse epidermis were isolated as described above. Real-time PCR was performed using the LightCycler system with FastStart DNA Master SYBR Green I to label amplified DNA (Roche). A standard curve method of quantification was used to calculate the expression of target genes relative to the housekeeping gene *β-actin*. Experiments were performed thrice. The following primer pairs were used for the PCR reactions: *Mrad9B*, 5′-CCCAAAAGACTATTTCCCAAG-3′ and 5′-TGTTCACAAGATACAGCTCCAA-3′; *p21*, 5′-GGAACATCTCAGGGCCGAAAA-3′ and 5′-GAGAGGGCAGGCAGCGTAT-3′; *p53*, 5′-CAGCACATGACGGAGGTCG-3′ and 5′-CTTCCAGATACTCGGGATACAA-3′; *β-actin*, 5′-GTAAAGACCTCTATGCCAACA-3′ and 5′-GGACTCATCGTACTCCTGCT-3′. PCR procedures for the these genes were template denaturation at 94°C for 5 min, then 40 cycles of 94°C for 15 s, 60°C for 20 s, 72.0 C for 13 s, and a final extension at 72°C for 3 min.

Western blotting. For preparing protein from epidermis, full-thickness skin removed from newborn mice was treated with 0.25% trypsin overnight at 4°C. The epidermis was peeled off from the dermis and dispersed in lysis buffer. To prepare cell lysate, keratinocytes incubated for 3 d were either left untreated or treated for 24 h with 0.15 μg/mL DMBA (Sigma). Then, the cell

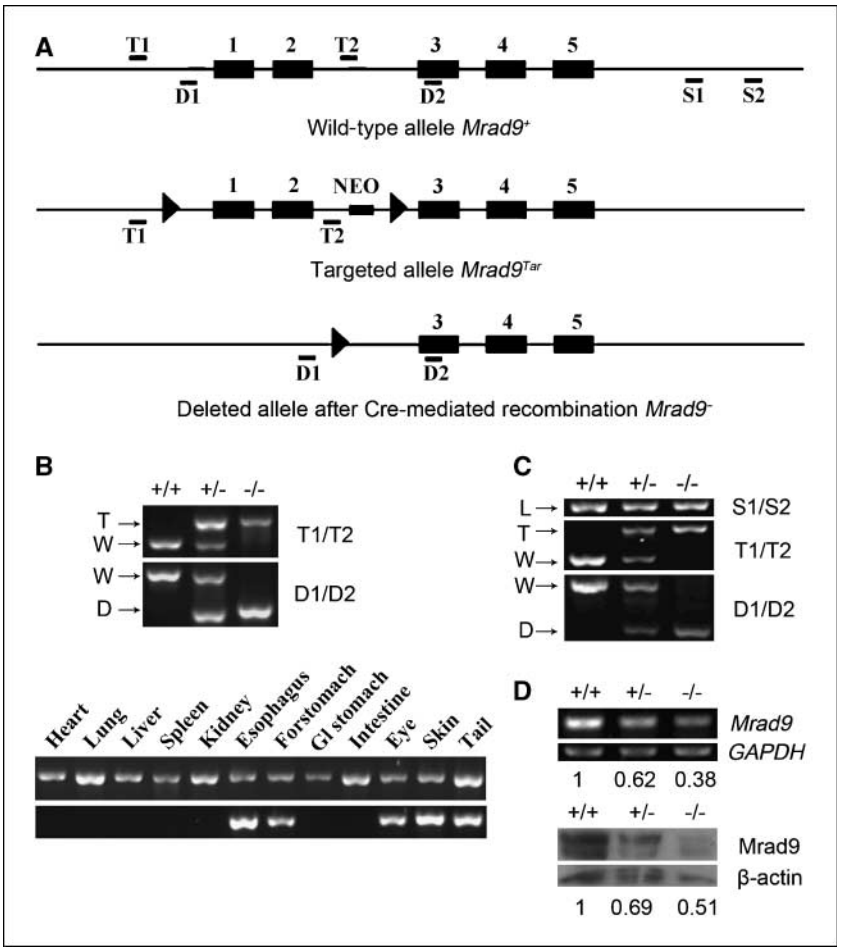

Figure 1. *Mrad9* deletion in keratinocytes. *A,* maps of original, targeted and deleted *Mrad9* genomic DNA fragments. *Black boxes,* exons; *thin lines,* introns as well as DNA sequences surrounding *Mrad9*. Locations of primer pairs for detecting the targeting (T1/T2), deletion (D1/D2) of the first two exons and DNA loading control (S1, S2) are marked. *B,* PCR genotyping of *Mrad9* deletion in mouse tissues. *Top,* results using primers T1/T2 and D1/D2, and mouse tail DNA as template. *Bottom,* the genotyping results using various mouse tissues. The deleted signature DNA band was only observed in tissues bearing keratinocytes. *gl stomach,* gland stomach. *C,* PCR-genotyping on skin keratinocytes incubated for 3 d after isolation. The PCR was semiquantitative and revealed the Cre efficiency to delete *Mrad9*. A PCR result using S1/S2 primers is given on the top as the DNA loading control. *D,* semiquantitative RT-PCR and Western blotting analyses for *Mrad9* mRNA and protein levels, respectively, of 1-d-old mouse pups. Quantitative comparisons to the wild-type are listed below the representative experimental results. +/+, +/−, and −/− represent $Mrad9^{+/+}$, $Mrad9^{+/-}$, and $Mrad9^{-/-}$ genotypes, respectively. W, T, D, and L on the left of PCR panels indicate signature bands of wild-type, targeted, deleted and loading control of *Mrad9*, respectively.

lysate was prepared in 1 × SDS-sample buffer, from a final concentration of 10^4 cells per microliter. Fifty micrograms of protein were resolved on a 10% SDS-PAGE gel, and proteins were transferred to a polyvinylidene difluoride membrane. The membrane was probed consecutively with primary and peroxidase-conjugated secondary antibodies, and the signal was detected using the SuperSignal West Pico Chemiluminescence Substrate system (Pierce). Primary and secondary antibodies used in this study are mouse anti–phospho-H2AX (Upstate), mouse anti-tubulin (Sigma), mouse anti-p21 (Santa Cruz), mouse anti-p53 (Oncogene), mouse anti-RAD9 (BD), rabbit anti-actin (Sigma), rabbit anti-RAD9B (prepared by Dr. Lieberman's laboratory), peroxidase-conjugated anti-mouse IgG (A9044; Sigma), and peroxidase-conjugated anti-rabbit IgG (A9169; Sigma).

DMBA-induced skin tumor formation. A published method, with minor modifications, was used to induce skin tumors in mice by the application of DMBA (17). The backs of mice (7- to 8-wk-old) were shaved 2 d before tumor induction. Then, one side of the shaved dorsal skin was painted with 2 μg DMBA (Sigma) in 0.1 mL acetone twice a week (Wednesday and Sunday); the other side was treated with only acetone as a control. Scoring for tumors was performed weekly. Positive tumor formation was determined using the following criteria: tumors 1 mm or larger in diameter were maintained for 2 wk. After positive identification of tumor formation, DMBA treatment was stopped. The longest painting was 25 wk, then the mice were observed for tumor formation for 5 more wk. All mice were also examined for the appearance of DMBA-induced pigment deposition spots. Criteria for the occurrence of pigment spots were detection of 10 or more spots, 1 mm or larger in diameter, on one side of the dorsal skin. In contrast, mice were considered pigmentation negative when no spots appeared or spots were smaller than 0.5 mm in diameter and fewer than 8 appeared. Overall, 70% of the negative mice contained no pigmentation spots.

Histologic analysis and immunohistochemistry. Dorsal skin samples and tumors were fixed in 4% paraformaldehyde at 4°C overnight, embedded in paraffin, and sectioned as 8-μm slices. The sectioned tissues on slides were stained with H&E (18, 19) or Van Gieson's (VG) Solution (20). Immunohistochemical staining was carried out using a kit (ImmunoCruz Staining Systems, Beijing Zhongshan Golden Bridge Biotechnology). The endogenous peroxidase activity in the specimens was blocked by treatment with 0.3% H_2O_2 and samples were then rinsed with PBS. The specimens were probed consecutively with primary antibodies against Keratin 14 (BAbCo), secondary antibody biotin-conjugated goat anti-rabbit IgG, and horseradish peroxidase–streptavidin complex, then visualized by diaminobenzidine. Afterwards, sections were counterstained with hematoxylin (18, 19).

PCR analysis of tumor and normal cells isolated by laser capture microdissection. Paraformaldehyde-fixed, paraffin-embedded tumors and normal skin tissues were sectioned and stained with H&E. To determine the status of *Mrad9* in presumably *Mrad9* nondeleted (*Tar/Tar*) or deleted (−/−) tumors, microdissection of tumor and adjacent normal cells from thin sections on slides was performed using a Leica laser microdissection system (Leica As LMD). Dissected cells were digested overnight with proteinase K. DNA isolation and PCR were carried out as described above.

Preparation and *in vitro* culture of keratinocytes. Full-thickness skin removed from newborn mice was treated with 0.25% trypsin overnight at 4°C. The epidermis was peeled off from the dermis and dispersed by stirring into single cells that were then suspended in Keratinocyte-SFM medium with supplements (Invitrogen). Cells were first incubated in dishes coated with collagen type I at 34°C in 5% CO_2 for 12 h to allow cells to attach to the bottom. Afterwards, unattached cells were removed by washing with PBS. Attached cells were further cultured in fresh medium, which was replaced every 2 d.

Proliferation assay. Keratinocytes were isolated as described and seeded into 12-well plates (3.5×10^5 cells per well) containing Keratinocyte-SFM medium with supplements. Cells were counted every 2 d. The effect of antioxidant treatment was assessed by culturing Keratinocytes in medium containing 1 μmol/L epigallocatechin gallate (EGCG) added initially on the second day of culturing, and included in the fresh medium used during routine maintenance of the cells.

Cell cycle analyses. The profile of cells in different phases of the cell cycle was determined using previously established methods (21). For a simple analysis of cell cycle distribution, 1×10^7 keratinocytes were plated per 10-cm dish. After incubation for 4 d, cells were processed and stained with propidium iodide (PI), then analyzed by a FACSCalibur (Becton Dickinson). To assess DNA synthesis, 10 μmol/L BrdUrd was added to medium and cells were pulse labeled for 40 min. Cells were then processed and probed with FITC-conjugated anti-BrdUrd antibody (Becton Dickinson) and stained with PI. Flow cytometric analyses were performed on a FACSCalibur.

Apoptosis assays. Keratinocytes, were cultured for 5 d and trypsinized for 10 min using 0.1% trypsin at 37°C (Sigma), washed twice with cold PBS, then resuspended in 1× binding buffer [10 mmol/L HEPES (pH 7.4), 140 mmol/L NaCl, and 2.5 mmol/L $CaCl_2$] at a concentration of 1×10^6 cells per milliliter. Then cells were stained with Annexin V-FITC (Jingmei Biotech) and PI for 15 min at room temperature, before flow cytometric analysis.

Neutral comet assay. Keratinocytes were first cultured in standard medium for 2 d, then incubated in medium containing 0, 0.01, 0.025, 0.05, or 0.1 μg/mL DMBA, respectively, for 24 h before analysis. The comet assay was carried out according to the manufacturer's instruction (Trevigen). Briefly, cells at a concentration of 1×10^5/mL were mixed gently with premelted low-temperature-melting agarose at a volume ratio of 1 to 10 (v/v) and spread on glass slides. The slides were then submerged in precooled neutral lysis buffer at 4°C for 30 min. After rinsing, the slides were equilibrated in Tris-borate EDTA solution, electrophoresed at 1.0 V/cm for 20 min, and then stained with PI. Fluorescence images for at least 50 nuclei were captured using a Nikon microscope and analyzed by CASP-1.2.2 software (University of Wroclaw) for tail moment (i.e., the geometric mean of fluorescence on the tail from the nucleus).

Statistical analysis. All statistical analyses were performed using statistical software package SAS Version 9.1.3 (22). The χ^2 test was used to compare genotype ratio for newborn pups derived from matings between $Mrad9^{+/-}$ mice. The Kaplan-Meier PL method (23) was used for comparison of the relative risks of tumor development induced by DMBA among the mice with the three *Mrad9* genotypes. We designed the tumor development experiment to meet a set of conditions so the Log-Rank Test in the Kaplan-Meier PL method could be used, and the number of animals used was reduced but results with statistical significance still could be achieved (refer to Results; ref. 24). The Student's t test was performed to determine statistical significance of the differences for the comet assay. In all the above analyses, a P value of <0.05 was considered statistically significant.

Results

Targeted deletion of *Mrad9* in mouse keratinocytes. $Mrad9^{-/-}$ mice die during embryonic development, but relative to wild-type controls, $Mrad9^{+/-}$ animals have no overt defects in gross morphology or health up to age 1.5 years (15). In this report, we describe the development of viable mice with a specific deletion of *Mrad9* in keratinocytes. These animals were made by crossing mice containing *loxP* targeted to *Mrad9* (15) with mice in which *Cre* transcription is under the control of the *K5* promoter, specifically activated in keratinocytes starting on day 14.5 dpc (16). After repeated backcrosses, homologous *Cre* genotypes were obtained in mice with three different *Mrad9* genotypes (Fig. 1*A* and *B*). *Cre* homozygous status of the mice was determined by crossing them with 2 mice bearing no *Cre*, which produced at least 15 *Cre*-positive pups and no *Cre*-negative pups (data not shown). Mating between $Cre^{+/+}$ $Mrad9^{Tar/+}$ mice yielded an offspring composition of $Mrad9^{+/+}$ (147): $Mrad9^{+/-}$ (245): $Mrad9^{-/-}$ (141), statistically equal to 1:2:1 (χ^2 Test: P = 0.845). Compared with animals with keratinocytes genetically $Mrad9^{+/+}$ or $Mrad9^{+/-}$, no obvious defects were observed in $Mrad9^{-/-}$ mice examined up to age 1.5 years (data not shown).

Deletion of *Mrad9* occurred exclusively in tissues (skin, forestomach, eye, and esophagus) that contain keratinocytes (Fig. 1*B*). Notably, PCR using DNA templates from $Cre^{+/+}$ $Mrad9^{Tar/Tar}$ mouse skin or isolated skin keratinocytes yielded both *Mrad9*-deleted as well as *Mrad9*-targeted signature bands (Fig. 1*B* and *C*), indicating that *Mrad9* deletion in skin keratinocytes was not complete, or there was a significant contamination of other types of cells. To exclude the possibility that the targeted signature bands mainly derived from contaminating nonkeratinocytes, the percentage of cells containing keratin 14 was assessed by flow cytometry. The isolated $Cre^{+/+}$ $Mrad9^{Tar/Tar}$ skin keratinocytes stained with anti–keratin 5 antibody were 96% keratin 14 positive (data not shown). We also reperformed the PCR using the T1/T2 primer pair and DNA templates from keratinocytes with 5 cycles less of reaction. For these conditions, the targeted signature bands were reduced to 1/9 and 1/18 in $Cre^{+/+}$ $Mrad9^{Tar/+}$ and $Cre^{+/+}$ $Mrad9^{Tar/Tar}$ keratinocytes, respectively; the wild-type signature band was not detected in the same PCR reaction (data not shown). However, the targeted signature band in $Cre^{+/+}$ $Mrad9^{Tar/Tar}$ cells was still 77% of that detected in $Cre^{+/+}$ $Mrad9^{Tar/+}$ cells. Taking all these data together, we conclude that a significant portion of skin keratinocytes did not have *Mrad9* deleted.

We also monitored *Mrad9* mRNA and protein levels in pup skins (Fig. 1*D*). RT-PCR analysis indicated that the *Mrad9/GADPH* mRNA ratios were 1, 0.62 and 0.38 in $Cre^{+/+}$ $Mrad9^{+/+}$, $Cre^{+/+}$ $Mrad9^{Tar/+}$, and $Cre^{+/+}$ $Mrad9^{Tar/Tar}$ skins, respectively. Western blotting illustrated that the Mrad9/β-actin protein level ratios were 1, 0.69, and 0.51 in wild-type, heterozygous, and homozygous cells, respectively. Thus, the Cre-mediated *Mrad9* deletion significantly lowered *Mrad9* expression in keratinocytes, and probably completely removed Mrad9 protein from a major portion of the $Cre^{+/+}$ $Mrad9^{Tar/Tar}$ keratinocyte population.

For descriptive purposes, $Mrad9^{+/+}$, $Mrad9^{+/-}$, and $Mrad9^{-/-}$ will be used to denote $Cre^{+/+}$ $Mrad9^{+/+}$, $Cre^{+/+}$ $Mrad9^{Tar/+}$, and $Cre^{+/+}$ $Mrad9^{Tar/Tar}$, respectively. However, as indicated by the results above, not all keratinocytes within the $Cre^{+/+}$ $Mrad9^{Tar/+}$ and $Cre^{+/+}$ $Mrad9^{Tar/Tar}$ cell populations were deleted for *Mrad9*.

Susceptibility of $Mrad9^{-/-}$ mice to skin tumorigenesis. To determine if *Mrad9* is important for tumorigenesis, the skin of mice with different status of *Mrad9* was smeared with DMBA. A total of 48 mice were divided into 3 groups, each with the $Mrad9^{+/+}$, $Mrad9^{+/-}$, or $Mrad9^{-/-}$ genotype, respectively. To increase the efficiency of the animal experiment statistically (24), we made a strict arrangement that the 3 groups of mice were from 16 litters,

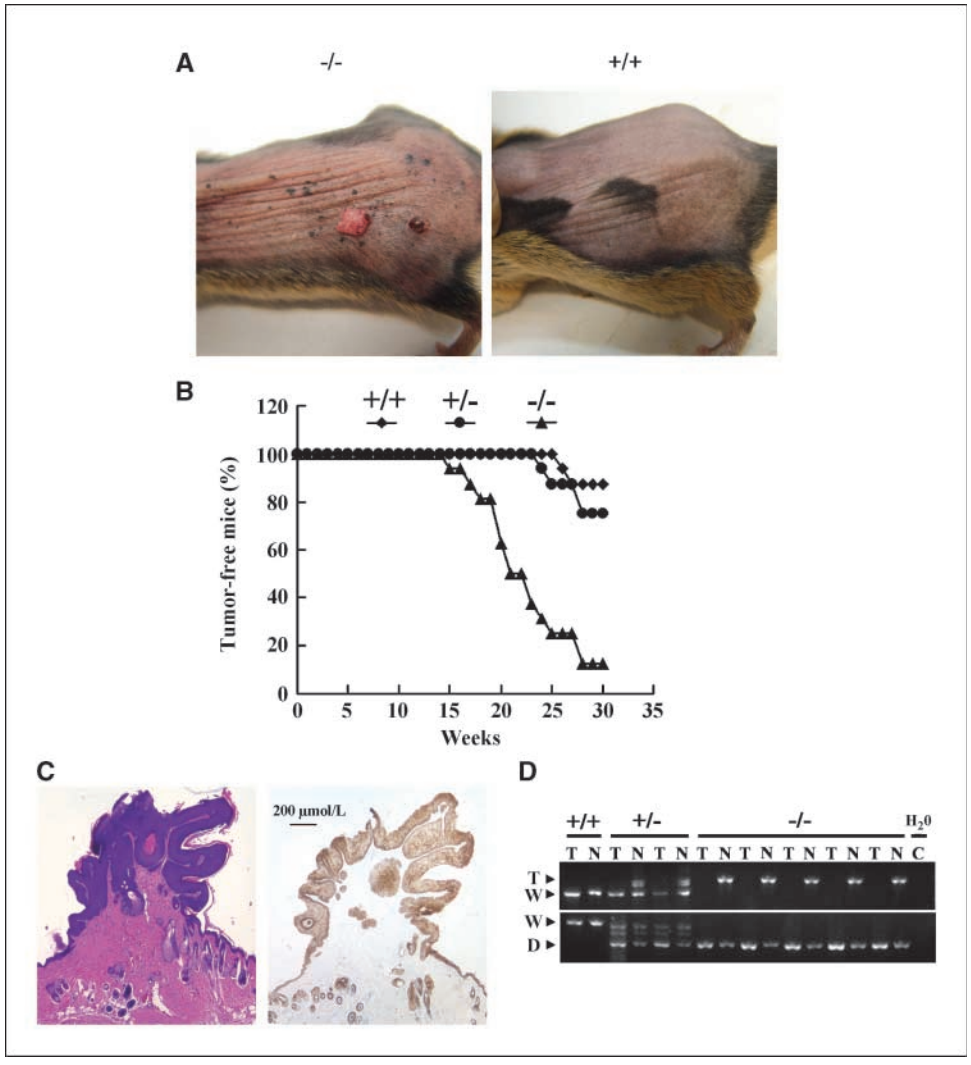

Figure 2. Skin tumor induction by DMBA. Forty eight mice were divided into three groups, each with the $Mrad9^{+/+}$ $Mrad9^{+/-}$ or $Mrad9^{-/-}$ genotype, respectively. The mice were subjected to DMBA treatment, and tumor development was examined. *A,* papillomas induced by DMBA treatment in $Mrad9^{-/-}$ mouse skin (*left*) and treated $Mrad9^{+/+}$ mouse control skin (*right*). *B,* incidence of induced tumor formation in mice of all three genotypes. Application of 2 μg DMBA/0.1 mL acetone onto skin started at ages 7 to 8 wk and was given twice a week. ♦, $Mrad9^{+/+}$; ●, $Mrad9^{+/-}$; ▲, $Mrad9^{-/-}$. *C,* H&E (*left*) staining illustrates a papilloma, with connective tissues extending into the tumor. The tissue is also stained for Keratin 14 (*right*), thus indicating that it is derived from keratinocytes. *D,* tumor cells and adjacent normal tissue cells were isolated and genotyped by PCR to reveal *Mrad9* status in the cells. +/+, +/−, and −/− represent $Mrad9^{+/+}$, $Mrad9^{+/-}$, and $Mrad9^{-/-}$ genotypes, respectively.

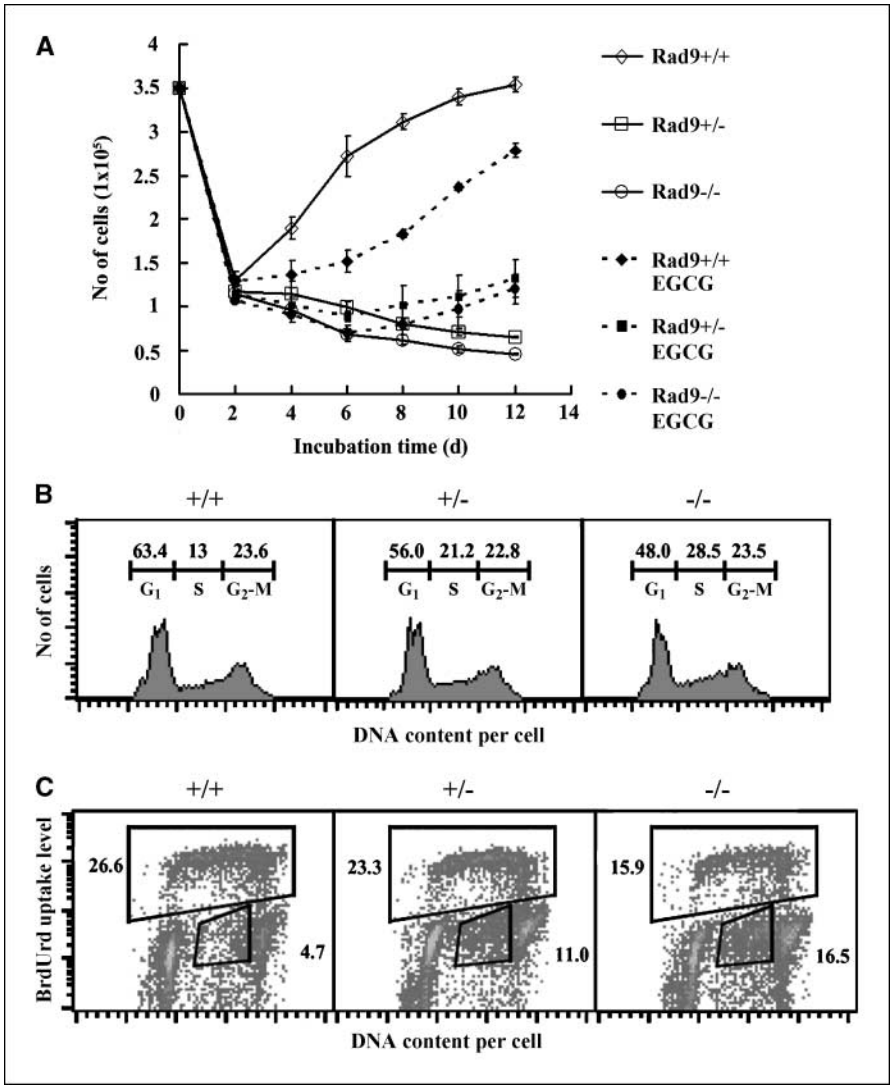

Figure 3. Proliferation and cell cycle distribution of wild-type and *Mrad9*-deficient keratinocytes in culture. *A,* proliferation of skin keratinocytes varying in *Mrad9* status. For cultures without EGCG: ◇, $Mrad9^{+/+}$; □, $Mrad9^{+/-}$; ○, $Mrad9^{-/-}$. Deletion of either one or two *Mrad9* loci retarded proliferation. For cultures with EGCG: ♦, $Mrad9^{+/+}$; ■, $Mrad9^{+/-}$; ●, $Mrad9^{-/-}$. The antioxidant EGCG was added to the medium. Retardation of *Mrad9*-deleted keratinocyte growth was alleviated by EGCG. *B,* flow cytometric analyses of cell cycle distributions of PI-stained keratinocytes with different *Mrad9* genotypes. Deletion of either one or two *Mrad9* loci led to reduced numbers of cells in G_1 and an increased number in S phase. The numbers above each phase indicate the percentage of cells in that phase among the whole cell population. *C,* flow cytometric analyses of keratinocytes stained with both PI and anti-BrdUrd. *Mrad9* status is indicated on the top. Fewer *Mrad9*-deficient cells were BrdUrd positive, and many of them were BrdUrd negative but contained a late S phase amount of DNA. The number in the top box is the percentage of BrdUrd-positive cells, and the number in the bottom right box is the percentage of BrdUrd-negative cells with late S phase DNA content.

each litter consisting of 3 mice with 3 different *Mrad9* genotypes, respectively, and identical sex, either female (10 liters) or male (6 liters). Under this setting, Log-Rank Test in the Kaplan-Meier PL method can be used for the statistical analysis on the significance of differences of tumor development among the three groups of animals (22, 23). DMBA is a chemical carcinogen that can induce tumors efficiently (25, 26). Two micrograms of DMBA in 0.1 mL acetone were painted onto shaved mouse skin twice a week for 25 weeks. Skin tumors began to appear on $Mrad9^{-/-}$ mouse skin after DMBA treatment for 15 weeks, whereas tumor onset occurred 25 and 27 weeks after the start of DMBA treatment in $Mrad9^{+/-}$ and $Mrad9^{+/+}$ mice, respectively (Fig. 2*A* and *B*). Staining skin specimens with H&E or antikeratin 14 showed that the tumors were derived from keratinocytes and possessed characteristics of papillomas (Fig. 2*C*; ref. 27). Kaplan-Meier PL method (23) was used for comparison of the relative hazards of tumor development induced by DMBA among the three genotypes of mice. The rate of tumor development in $Mrad9^{-/-}$ mice was significantly higher than in $Mrad9^{+/-}$ and $Mrad9^{+/+}$ animals ($P = 0.0004$ and $P = 0.0003$, respectively, Log-Rank Test). Although $Mrad9^{+/-}$ mice tended to be more prone to induced tumorigenicity than $Mrad9^{+/+}$ mice, the difference is not statistically significant ($P = 0.4088$, Log-Rank Test). Therefore, lower levels of Mrad9 caused by haploinsufficiency did not cause significantly increased cancer development, relative to wild-type controls.

Because the Cre-mediated *Mrad9* deletion was not complete, to confirm the importance of *Mrad9* in tumor inhibition, tumor and nearby normal cells were isolated using laser capture microdissection, and their genomic DNA was subjected to PCR. All five examined tumors from $Mrad9^{-/-}$ mice were $Mrad9^{-/-}$, whereas the normal cells on the sides of the tumors still contained undeleted but targeted *Mrad9* (Fig. 2*D*) as expected, indicating that Mrad9 indeed plays a significant role in preventing tumor development.

Under this experimental setting, the number of induced tumors for all three *Mrad9* genotypes was 1 or 2, and differences between mice with different *Mrad9* genotypes were not observed.

***Mrad9* deletion alters the cell cycle profile of keratinocytes and increases DNA damage.** Because Rad9 plays important roles in DNA repair and cell cycle checkpoint controls, two processes important for maintaining genomic integrity and preventing carcinogenesis, we investigated these processes in keratinocytes bearing an *Mrad9* deletion. Skin keratinocytes were isolated from 1-day-old pups. The cells were grown in defined Keratinocyte-SFM

medium (Life Technologies, Inc.). The number of cells with each of the three genotypes dropped to <30% of the seeded (3.5×10^5 per well) level after the first 2 days of incubation. Subsequently, the total number of wild-type cells increased between day 2 and 6, then cell proliferation slowed down (Fig. 3*A*; data not shown). In contrast, the total number of *Mrad9*$^{-/-}$ cells continued to decrease (Fig. 3*A*; data not shown). The *Mrad9*$^{-/-}$ cells did not stop decreasing in number and did not begin to grow after extended culturing (data not shown). There were two types of *Mrad9* heterozygous pups when mouse tail DNA was used for genotyping 1 day after birth, one with a high frequency of deletion of the *Mrad9*-targeted allele and the other with a low level of deletion (PCR data not shown). However, when genotyped again in 20-day and 2-month-old mice, there was only the latter type of deletion (data not shown). Furthermore, the cells isolated from all newborn *Mrad9*$^{+/-}$ pups were found to have the latter deletion type after being cultured 3 days and then genotyped. The reason for having the subtle differences among newborn *Mrad9*$^{+/-}$ pups was not understood, but for the succinctness of experiments, the differences were not distinguished for the rest of the study.

We tested whether reduction in number of *Mrad9*-deleted keratinocytes was caused by DNA lesions induced by reactive oxygen species (ROS) because it is known that Rad9 plays an important role in DNA damage repair. Conventionally, cells are cultured at 20% O_2. Incubation at this O_2 concentration loads cells with a higher O_2 tension (thus higher ROS level) than within animals (28–30). We used the antioxidant EGCG to scavenge oxidative-free radicals to assess the effect of the high oxygen tension present during cell culture, relative to *in vivo* in the animal, on cell proliferation. The addition of 1 μmol/L of the antioxidant EGCG to the medium changed the direction of the cell growth curves of *Mrad9*$^{-/-}$ and *Mrad9*$^{+/-}$ keratinocytes upward from day 6 (Fig. 3*A*). Therefore, high O_2 tension was a major cause for the cell number reduction observed. Growth of the wild-type cells also slowed down in the EGCG-containing medium, an established inhibitory effect of the drug on cell proliferation (31, 32).

Flow cytometric analyses of PI-stained keratinocytes indicated that more *Mrad9*$^{-/-}$ and *Mrad9*$^{+/-}$ cells, compared with the wild-type controls, accumulated in late S phase (Fig. 3*B*). A measurement of BrdUrd uptake by replicative S phase cells in combination with DNA content via PI staining in individual cells can reveal more information on cell cycle distribution. Therefore, we investigated cell cycle profiles in more detail by pulse labeling with BrdUrd and staining cells after 4 days of incubation. A major population of *Mrad9*$^{-/-}$ and *Mrad9*$^{+/-}$ cells with DNA content in the range primarily of late S phase was not labeled by BrdUrd, and there were fewer BrdUrd-positive *Mrad9*$^{-/-}$ and *Mrad9*$^{+/-}$ cells than wild-type cells in S phase (Fig. 3*C*). The BrdUrd-negative cells with late S phase DNA content means that the cells were arrested in late S phase. Based on the above data, we conclude that the arrest of cells in late S phase is an important cause for the cell

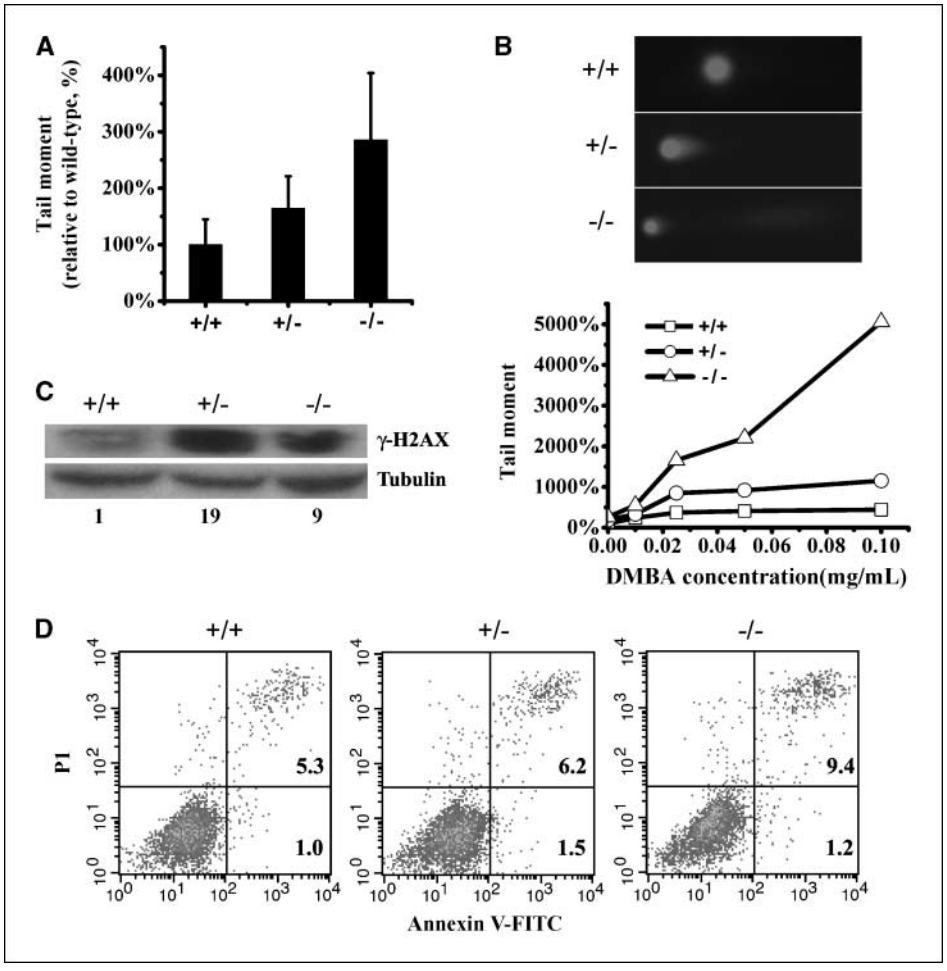

Figure 4. Spontaneous and DMBA-induced DNA DSBs and apoptosis. *A,* evaluation of spontaneous DNA DSBs in keratinocytes by the neutral comet assay. Cells were incubated for 3 d before collection and analysis. Both *Mrad9*$^{+/-}$ and *Mrad9*$^{-/-}$ cells contained significantly more DSBs ($P = 1.4 \times 10^{-6}$ and $P = 3.0 \times 10^{-17}$, respectively) compared with the wild-type control. *B,* to evaluate DMBA-induced DNA DSBs in keratinocytes, cells were first incubated for 48 h, then different concentrations of DMBA were added to the cells, which were subsequently cultured for an additional 24 h. DMBA (0.1 μg/mL) induced apoptosis in *Mrad9*$^{-/-}$ cells as indicated by the prolonged tail but not in the cells with the two other genotypes (*top*). *C,* Western blotting analysis of γ-H2AX levels without DMBA treatment. Lysates were prepared from cells incubated for 3 d after initial isolation. The relative quantitative comparison of γ-H2AX levels of the three cell types is illustrated at the bottom of the panel (1:19:9). *D,* flow cytometric analysis of keratinocytes to assess spontaneous apoptosis using Annexin V labeling. Cells were incubated for 4 d before harvesting for apoptotic analysis. +/+, +/−, and −/− represent *Mrad9*$^{+/+}$, *Mrad9*$^{+/-}$, and *Mrad9*$^{-/-}$ genotypes, respectively.

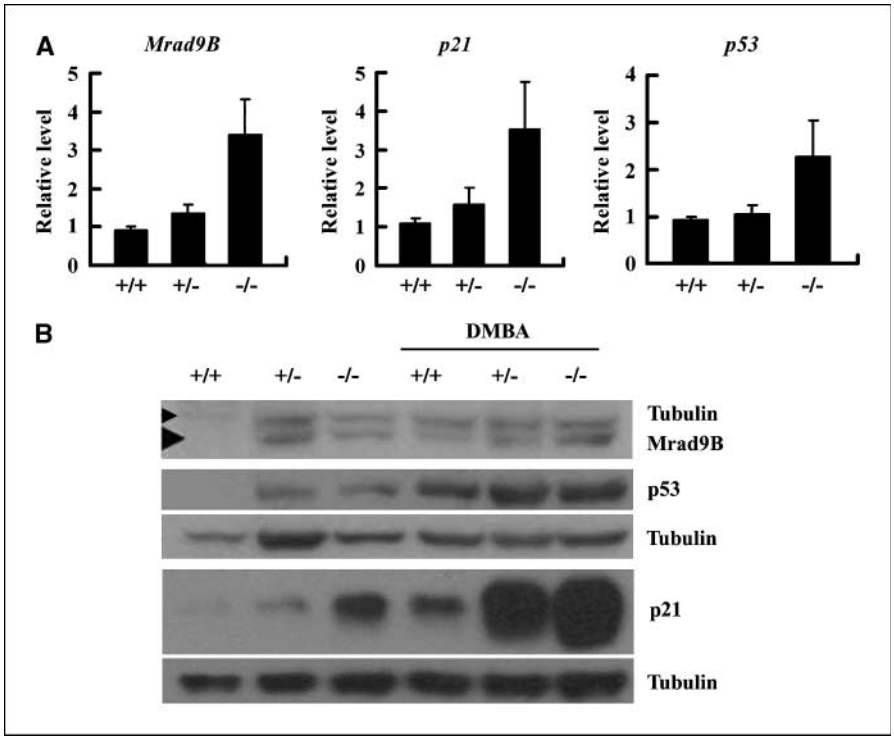

Figure 5. Expression of *Mrad9B, p21*, and *p53* in keratinocytes differing in *Mrad9* status. *A,* real-time quantitative RT-PCR analysis of *Mrad9B, p21*, and *p53* mRNA levels in 1-d-old mouse skin. Status of *Mrad9* is indicated. Each relative level is the average ratio of the PCR results of an indicated gene relative to β-*actin* for three independent samples, and each PCR result is the mean of triplet PCR of the same sample. *B,* Western blotting analysis of Mrad9B, p21, and p53 protein levels in keratinocytes incubated for 3 d after initial isolation. The first three lanes are the protein levels in cells without DMBA treatment, and the last three lanes are the protein levels in cells treated with 0.15 μg/mL DMBA for 24 h. The data in the figure are three representative Western blotting results, and each has an independent tubulin control. +/+, +/−, and −/− represent $Mrad9^{+/+}$, $Mrad9^{+/-}$, and $Mrad9^{-/-}$ genotypes, respectively.

number reduction of $Mrad9^{-/-}$ and $Mrad9^{+/-}$ keratinocytes during *in vitro* incubation.

We used the neutral comet assay to detect double-strand breaks (DSBs) in DNA. There were significantly more DSBs in incubated $Mrad9^{+/-}$ cells than in wild-type cells, and more DSBs in $Mrad9^{-/-}$ cells than in $Mrad9^{+/-}$ cells (Fig. 4*A*). Therefore, *Mrad9* is critical for maintaining genomic integrity, and there is a dosage-dependent effect. H2AX phosphorylation level is another established indicator of DNA DSBs. Consistent with the comet assay results, H2AX phosphorylation levels from lysates of $Mrad9^{-/-}$ cells as well as $Mrad9^{+/-}$ cells were much higher than in wild-type cell lysates (Fig. 4*C*). Interestingly, H2AX phosphorylation level from $Mrad9^{-/-}$ cells (arbitrary number 9) was lower than that from $Mrad9^{+/-}$ cells (arbitrary number 19). H2AX phosphorylation occurs predominantly in S phase and G_2-M phase cells during *in vitro* culturing (33). The lower ratio of normal S phase cells is likely a cause for the relatively lower H2AX phosphorylation level compared with that of $Mrad9^{+/-}$ cells (Fig. 3*C*). In spite of possible influence by the changed cell cycle distribution, the overall H2AX phosphorylation level in $Mrad9^{-/-}$ cells was still higher than that in wild-type cells (arbitrary number 1).

As we showed above, tumors only appeared after DMBA treatment. Therefore, we asked if DMBA treatment causes more DSBs in *Mrad9*-deficient cells than in wild-type cells. As predicted, incubation in medium containing 0.02 to 0.05 μg/mL DMBA induced significantly more DSBs in *Mrad9*-deficient cells than in wild-type cells (Fig. 4*B*). Further increase in the DMBA concentration to 0.1 μg/mL greatly enhanced tail moment and coefficient variance of tail moment in the $Mrad9^{-/-}$ cells. The dramatic increases in both tail moment and its coefficient variance were because a subpopulation of $Mrad9^{-/-}$ cells had very long tails (Fig. 4*B*; data not shown), a characteristic of apoptosis (34). No apoptosis was observed in $Mrad9^{+/-}$ and $Mrad9^{+/+}$ cells treated with DMBA.

To confirm the effects of *Mrad9* deletion on apoptosis, we stained the same cell populations for Annexin V-FITC and PI to provide supporting evidence. We found that the percentage of apoptotic cells among $Mrad9^{+/-}$ keratinocytes (7.74%) was higher than that of $Mrad9^{+/+}$ cells (6.32%). The percentage of $Mrad9^{-/-}$ apoptotic cells (10.58%) was higher than that of $Mrad9^{+/-}$ cells (Fig. 4*D*). The inhibitory effect of Rad9 on apoptosis was consistent with previously reported effects on murine embryonic stem cells (35) and chicken DT40 cells (36).

Effect of *Mrad9* deletion on expression of other cell cycle checkpoint genes. Expression of other cell cycle checkpoint genes, including *p21, p53*, and *Rad9B*, in $Mrad9^{-/-}$ and control keratinocytes was assessed by quantitative RT-PCR and Western blotting to gain mechanistic insight into the function of *Mrad9*. Both heterozygous and homozygous deletion of *Mrad9* induced expression of *p21, p53*, and *Rad9B* in skin keratinocytes (Fig. 5*A* and *B*). Statistical analyses on the quantitative RT-PCR results indicate that the expression of the three genes in $Mrad9^{-/-}$ cells is significantly higher than those in $Mrad9^{+/-}$ and $Mrad9^{+/+}$ cells (Fig. 5*A*). DMBA treatment (0.15 μg/mL, 24 h) increased the levels of p21 and p53 proteins in cells with each of the three genotypes (Fig. 5*B*). The same treatment also enhanced Mrad9B protein level in wild-type cells but not obviously in $Mrad9^{-/-}$ and $Mrad9^{+/-}$ cells. These results suggest that the genomic DNA damage stress response system is increased in cells with a deletion of *Mrad9*.

Susceptibility of $Mrad9^{-/-}$ mice to the development of aging skin. In the same set of mice used for tumor development experiments, DMBA treatment to skin readily induced skin pigment deposition in $Mrad9^{-/-}$ mice (Fig. 5*A*). Within the DMBA treatment experimental period (30 weeks), skin pigment deposition occurred on 81.3% of $Mrad9^{-/-}$, 25% of $Mrad9^{+/-}$, and 12.5% of $Mrad9^{+/+}$ mice (Fig. 5*B*). Pigment deposition occurred in 2 to 5 weeks after tumor formation in most mice and after the end of DMBA treatment in mice bearing any of the three genotypes (data

not shown). H&E and VG staining on skin specimens showed that pigment particles in the dermis were abnormally increased (Fig. 5*C* and *D*), hair follicle number significantly decreased, and epidermis atrophied in *Mrad9*$^{-/-}$ mice. These phenotypes indicate that the skin of *Mrad9*$^{-/-}$ mice aged readily in response to DMBA treatment. However, the phenotypes did not appear without DMBA treatment (data not shown), suggesting that they are mediated by DNA damage.

Discussion

The *Rad9* gene is evolutionarily conserved from yeast to human and critical for cell cycle checkpoint controls as well as DNA repair (6, 7). Its role as a tumor suppressor has not been reported thus far, although many DNA repair and cell cycle checkpoint genes are required for preventing tumorigenesis. Here, we report the establishment of a conditional *Mrad9* knockout model using mouse keratinocytes to examine whether *Mrad9* is inhibitory to tumor formation and the mechanisms involved (Fig. 1). We showed that *Mrad9* is required for suppressing skin tumor formation induced by the DNA-damaging agent DMBA (Fig. 2). Furthermore, we show that *Mrad9* also plays a key role in preventing skin aging induced by DMBA treatment (Fig. 6).

Although DMBA treatment enhanced the incidence of papillomas in *Mrad9* deleted skin keratinocytes statistically significantly more than in wild-type keratinocytes, the *Mrad9* deletion alone did not lead to an increase in spontaneous tumor formation. DNA repair, cell cycle checkpoint controls, and apoptosis are three key

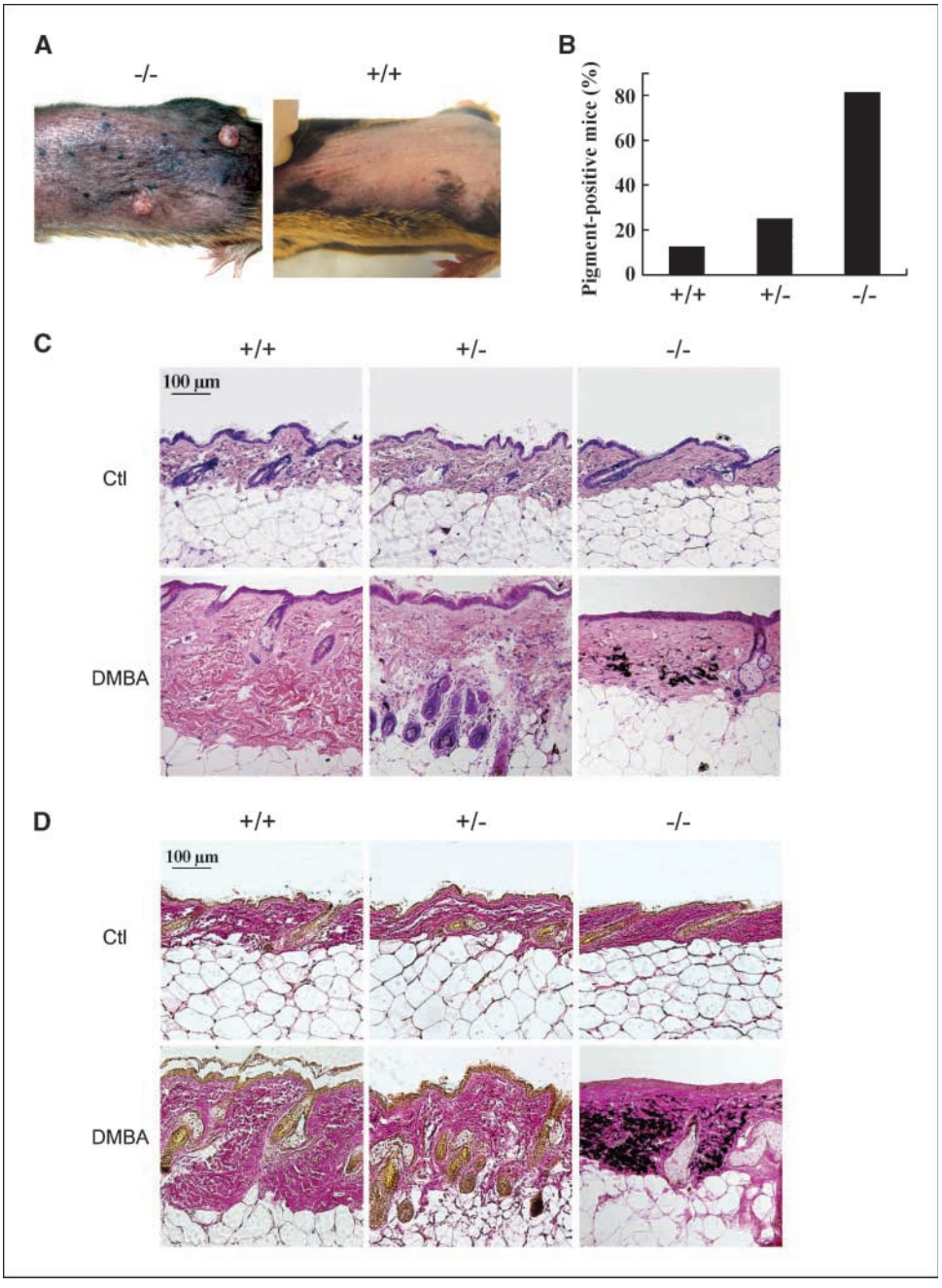

Figure 6. DMBA-induced skin aging in wild-type or *Mrad9*-deleted mice. *A,* *Mrad9*$^{-/-}$ (*left*) and *Mrad9*$^{+/+}$ (*right*) mice shown were treated with DMBA for 25 wk. *B,* skin pigment deposition in mice with different *Mrad9* status treated with DMBA. *C,* H&E staining of DMBA-treated mouse skins. DMBA caused a reduction of follicles, atrophied skin, and abnormal pigment deposition on *Mrad9*$^{-/-}$ mouse skin, whereas DMBA-treated skins of *Mrad9*$^{+/+}$ and *Mrad9*$^{+/-}$ mice looked normal. *D,* VG staining of DMBA-treated skin. This treatment led to a thinner but dense dermis in *Mrad9*$^{-/-}$ but not in *Mrad9*$^{+/+}$ or *Mrad9*$^{+/-}$ mouse skins. +/+, +/−, and −/− represent *Mrad9*$^{+/+}$, *Mrad9*$^{+/-}$, and *Mrad9*$^{-/-}$ genotypes, respectively. *Ctl,* control.

functions in preventing the formation of primary tumors. There is an abundance of evidence indicating that Rad9 participates in multiple DNA repair pathways (8, 37–43) and cell cycle checkpoints (15, 44–46). Both antiapoptotic and proapoptotic roles were reported using different human and animal cell lines (36, 47–49). The roles of Rad9 in DNA repair and apoptosis in keratinocytes have not been reported previously. We illustrated in this study that keratinocytes with *Mrad9* deleted at either one or two loci had more DNA DSBs, and the increase of DNA lesions induced by DMBA was more significant in *Mrad9*-deleted cells than in wild-type controls (Fig. 4). Therefore, the function of *Mrad9* in repairing DNA lesions is likely one key component of the ability of the protein to repress tumorigenesis. *Mrad9* deletion led to higher apoptotic keratinocytes in culture either with DMBA treatment or not (Fig. 4*C*), thus, apoptosis is not a significant mechanism used by *Mrad9* to serve as a gatekeeper to prevent tumor formation in skin keratinocytes.

Human Rad9 protein can bind the *p21* promoter region and induce *p21* transcription (50). Here, we showed that *Mrad9* deletion highly enhanced *p21* expression (Fig. 5*A*). However, *Mrad9* deletion also induced *p53* expression (Fig. 5*A*), which could serve as the transactivator of *p21* expression. Interestingly, *Mrad9* deletion also enhanced *Mrad9B* (*Mrad9* homologue) expression. Because *Mrad9* deletion alone did not lead to tumor formation, it is possible that *Mrad9B* might have at least partially redundant functions related to *Mrad9* activity. Treatment with DMBA increased Mrad9B protein level in wild-type keratinocytes but did not further enhance Mrad9B level in $Mrad9^{-/-}$ and $Mrad9^{+/-}$ keratinocytes. However, DMBA treatment increased p21 and p53 protein levels in keratinocytes with any of the three *Mrad9* genotypes (Fig. 5*B*). The Mrad9B level seems to be limited to relatively low abundance compared with p21 and p53 levels, suggesting that the regulation of Mrad9B is different from that of p21 and p53.

DMBA treatment also caused mouse skin aging in *Mrad9*-deleted animals more significantly than in wild-type controls. Skin aging was reflected as increased pigmentation, decreased hair follicles, and atrophied epidermis. In cell culture, *Mrad9*-deleted keratinocytes have more DSBs and a net negative growth (Fig. 4*A*). Detailed examination revealed that many *Mrad9*-deficient cells were arrested in late S phase and more tended to go into apoptosis (Figs. 3*D* and 4*C*). The *Mrad9*-deficient cells did not stop replicating, thus the arrest in late S phase and apoptosis are major contributing factors to the negative growth of *Mrad9*-deleted keratinocytes cultured *in vitro*. The negative growth was reversed by addition of the antioxidant EGCG to the medium (Fig. 3*A*), suggesting that oxidative free radicals lead to the growth defect, probably due to an enhancement in the frequency of DNA lesions. Under *in vivo* conditions where oxygen tension is lower and keratinocytes are in a more compatible environment, it is conceivable that extra genomic stress such as DMBA treatment is needed to increase the number of DNA lesions and mediate the proliferation defect.

It is clear from our results that Rad9 affects cell cycle distribution in keratinocytes. How Mrad9 regulates cell cycle checkpoints in keratinocytes and the relationship to the mechanism that arrests *Mrad9*-deleted keratinocytes in late S phase remain to be addressed. The mechanism underlying the latter novel phenotype, in particular, is worth further investigation.

In summary, we show that Rad9 is important for resisting the development of tumors in keratinocytes, and roles in several molecular mechanisms that stabilize the genome might be involved. This work underscores the need to understand the function of Rad9 and other cell cycle checkpoint or DNA repair proteins, especially in terms of their effect on tumorigenesis and potential for translational effect in the clinic.

Disclosure of Potential Conflicts of Interest

No potential conflicts of interest were disclosed.

Acknowledgments

Received 9/27/2007; revised 3/6/2008; accepted 4/16/2008.

Grant support: National Natural Science Foundation of China 30470373 and 30530180 (H. Hang), National Protein Project of Ministry of Science and Technology 2006CB910902 (H. Hang), Knowledge Innovation Program of Chinese Academy of Sciences KSCX2-YW-R63 (H. Hang), and NIH grants GM079107 and CA130536 (H.B. Lieberman).

The costs of publication of this article were defrayed in part by the payment of page charges. This article must therefore be hereby marked *advertisement* in accordance with 18 U.S.C. Section 1734 solely to indicate this fact.

We thank Dr. Songmei Geng, Department of Dermatology, Second Hospital, Xi'An JiaoTong University, China for helpful discussions and suggestions on histologic analysis; Dr. Jianhua Liu, Department of Health Statistics, Chinese Centers for Disease Control and Prevention, China for statistical analyses; and Dr. Xiao Liang, State Key Laboratory of Molecular Oncology, Cancer Institute/Cancer Hospital, Chinese Academy of Medical Sciences and Peking Union Medical College, China for technical assistance related to laser capture microdissection.

References

1. Miki Y, Swensen J, Shattuck-Eidens D, et al. A strong candidate for the breast and ovarian cancer susceptibility gene BRCA1. Science 1994;266:66–71.
2. Deng CX. BRCA1: cell cycle checkpoint, genetic instability, DNA damage response and cancer evolution. Nucleic Acids Res 2006;34:1416–26.
3. Levine AJ, Momand J, Finlay CA. The p53 tumour suppressor gene. Nature 1991;351:453–6.
4. Houtgraaf JH, Versmissen J, van der Giessen WJ. A concise review of DNA damage checkpoints and repair in mammalian cells. Cardiovasc Revasc Med 2006;7:165–72.
5. Shiloh Y. ATM and related protein kinases: safeguarding genome integrity. Nat Rev 2003;3:155–68.
6. Parrilla-Castellar ER, Arlander SJ, Karnitz L. Dial 9–1-1 for DNA damage: the Rad9–1-Rad1 (9–1-1) clamp complex. DNA Repair (Amst) 2004;3:1009–14.
7. Lieberman HB. Rad9, an evolutionarily conserved gene with multiple functions for preserving genomic integrity. J Cell Biochem 2006;97:690–7.
8. Toueille M, El-Andaloussi N, Frouin I, et al. The human Rad9/Rad1/Hus1 damage sensor clamp interacts with DNA polymerase β and increases its DNA substrate utilisation efficiency: implications for DNA repair. Nucleic Acids Res 2004;32:3316–24.
9. Maniwa Y, Yoshimura M, Bermudez VP, et al. Accumulation of hRad9 protein in the nuclei of nonsmall cell lung carcinoma cells. Cancer 2005;103:126–32.
10. Cheng CK, Chow LW, Loo WT, Chan TK, Chan V. The cell cycle checkpoint gene Rad9 is a novel oncogene activated by 11q13 amplification and DNA methylation in breast cancer. Cancer Res 2005;65:8646–54.
11. Maniwa Y, Yoshimura M, Bermudez VP, et al. His239Arg SNP of HRAD9 is associated with lung adenocarcinoma. Cancer 2006;106:1117–22.
12. Wang L, Hsu CL, Ni J, et al. Human checkpoint protein hRad9 functions as a negative coregulator to repress androgen receptor transactivation in prostate cancer cells. Mol Cell Biol 2004;24:2202–13.
13. Zhu A, Zhang X, Lieberman HB. Rad9 has a functional role in human prostate carcinogenesis. Cancer Res 2008;68:1267–74.
14. Smilenov LB, Lieberman HB, Mitchell SA, Baker RA, Hopkins KM, Hall EJ. Combined haploinsufficiency for ATM and RAD9 as a factor in cell transformation, apoptosis, and DNA lesion repair dynamics. Cancer Res 2005;65:933–8.
15. Hopkins KM, Auerbach W, Wang XY, et al. Deletion of mouse rad9 causes abnormal cellular responses to DNA damage, genomic instability, and embryonic lethality. Mol Cell Biol 2004;24:7235–48.
16. Mao CM, Yang X, Cheng X, Lu YX, Zhou J, Huang CF. [Establishment of keratinocyte-specific Cre recombinase transgenic mice]. Yi Chuan Xue Bao 2003;30:407–13.
17. Hirao A, Cheung A, Duncan G, et al. Chk2 is a tumor suppressor that regulates apoptosis in both an ataxia

telangiectasia mutated (ATM)-dependent and an ATM-independent manner. Mol Cell Biol 2002;22:6521–32.
18. Yang L, Mao C, Teng Y, et al. Targeted disruption of Smad4 in mouse epidermis results in failure of hair follicle cycling and formation of skin tumors. Cancer Res 2005;65:8671–8.
19. Suzuki A, Itami S, Ohishi M, et al. Keratinocyte-specific Pten deficiency results in epidermal hyperplasia, accelerated hair follicle morphogenesis and tumor formation. Cancer Res 2003;63:674–81.
20. Culling CFA. Handbook of histopathological and histochemical techniques. 3rd ed. London: Butterworth; 1974.
21. Hang HYFM. Analysis of the mammalian cell cycle by flow cytometry. In: Lieberman HB, editor. Cell cycle checkpoint control protocols. Totowa (NJ): Humana Press; 2004.
22. SAS Institute Inc. SAS/STAT®9.1 User's Guide: Cary (NC): SAS Institute Inc.; 2004.
23. Lee ET, Wang JW. Statistical Methods for Survival Data Analysis. 3rd ed. New York: John Wiley and Sons; 2003.
24. Michael FW, Festing PO, Das RG, Borja MC, Berdoy M. The Design of Animal Experiments. Reducing the use of animals in research through better experimental design. Laboratory Animal Handbooks NO. 14. London: The Royal Society of Medicine Press Ltd; 2002.
25. Quintanilla M, Brown K, Ramsden M, Balmain A. Carcinogen-specific mutation and amplification of Ha-ras during mouse skin carcinogenesis. Nature 1986;322:78–80.
26. Corominas M, Leon J, Kamino H, Cruz-Alvarez M, Novick SC, Pellicer A. Oncogene involvement in tumor regression: H-ras activation in the rabbit keratoacanthoma model. Oncogene 1991;6:645–51.
27. Knutsen GL, Kovatch RM, Robinson M. Gross and microscopic lesions in the female SENCAR mouse skin and lung in tumor initiation and promotion studies. Environ Health Perspect 1986;68:91–104.
28. Knighton DR, Hunt TK, Scheuenstuhl H, Halliday BJ, Werb Z, Banda MJ. Oxygen tension regulates the expression of angiogenesis factor by macrophages. Science 1983;221:1283–5.
29. Chen Q, Fischer A, Reagan JD, Yan LJ, Ames BN. Oxidative DNA damage and senescence of human diploid fibroblast cells. Proc Natl Acad Sci U S A 1995;92:4337–41.
30. Saito H, Hammond AT, Moses RE. The effect of low oxygen tension on the *in vitro* -replicative life span of human diploid fibroblast cells and their transformed derivatives. Exp Cell Res 1995;217:272–9.
31. Yang GY, Liao J, Kim K, Yurkow EJ, Yang CS. Inhibition of growth and induction of apoptosis in human cancer cell lines by tea polyphenols. Carcinogenesis 1998;19:611–6.
32. Ahmad N, Feyes DK, Nieminen AL, Agarwal R, Mukhtar H. Green tea constituent epigallocatechin-3-gallate and induction of apoptosis and cell cycle arrest in human carcinoma cells. J Natl Cancer Inst 1997;89:1881–6.
33. Tanaka T, Kurose A, Huang X, Traganos F, Dai W, Darzynkiewicz Z. Extent of constitutive histone H2AX phosphorylation on Ser-139 varies in cells with different TP53 status. Cell Prolif 2006;39:313–23.
34. Yasuhara S, Zhu Y, Matsui T, et al. Comparison of comet assay, electron microscopy, and flow cytometry for detection of apoptosis. J Histochem Cytochem 2003;51:873–85.
35. Zhu A, Zhou H, Leloup C, et al. Differential impact of mouse Rad9 deletion on ionizing radiation-induced bystander effects. Radiat Res 2005;164:655–61.
36. Delacroix S, Wagner JM, Kobayashi M, Yamamoto K, Karnitz LM. The Rad9–Hus1-Rad1 (9–1-1) clamp activates checkpoint signaling via TopBP1. Genes Dev 2007;21:1472–7.
37. Smirnova E, Toueille M, Markkanen E, Hubscher U. The human checkpoint sensor and alternative DNA clamp Rad9–1-Hus1 modulates the activity of DNA ligase I, a component of the long-patch base excision repair machinery. Biochem J 2005;389:13–7.
38. Pandita RK, Sharma GG, Laszlo A, et al. Mammalian Rad9 plays a role in telomere stability, S- and G2-phase-specific cell survival, and homologous recombinational repair. Mol Cell Biol 2006;26:1850–64.
39. Brandt PD, Helt CE, Keng PC, Bambara RA. The Rad9 protein enhances survival and promotes DNA repair following exposure to ionizing radiation. Biochem Biophys Res Commun 2006;347:232–7.
40. Guan X, Bai H, Shi G, et al. The human checkpoint sensor Rad9–1-Hus1 interacts with and stimulates NEIL1 glycosylase. Nucleic Acids Res 2007;35:2463–72.
41. Wang W, Lindsey-Boltz LA, Sancar A, Bambara RA. Mechanism of stimulation of human DNA ligase I by the Rad9–1-Hus1 checkpoint complex. J Biol Chem 2006;281:20865–72.
42. Wang W, Brandt P, Rossi ML, et al. The human Rad9–1-Hus1 checkpoint complex stimulates flap endonuclease 1. Proc Natl Acad Sci U S A 2004;101:16762–7.
43. Shi G, Chang DY, Cheng CC, Guan X, Venclovas C, Lu AL. Physical and functional interactions between MutY glycosylase homologue (MYH) and checkpoint proteins Rad9–1-Hus1. Biochem J 2006;400:53–62.
44. Chen MJ, Lin YT, Lieberman HB, Chen G, Lee EY. ATM-dependent phosphorylation of human Rad9 is required for ionizing radiation-induced checkpoint activation. J Biol Chem 2001;276:16580–6.
45. Kobayashi M, Hirano A, Kumano T, et al. Critical role for chicken Rad17 and Rad9 in the cellular response to DNA damage and stalled DNA replication. Genes Cells 2004;9:291–303.
46. Dang T, Bao S, Wang XF. Human Rad9 is required for the activation of S-phase checkpoint and the maintenance of chromosomal stability. Genes Cells 2005;10:287–95.
47. Yoshida K, Komatsu K, Wang HG, Kufe D. c-Abl tyrosine kinase regulates the human Rad9 checkpoint protein in response to DNA damage. Mol Cell Biol 2002;22:3292–300.
48. Yoshida K, Wang HG, Miki Y, Kufe D. Protein kinase Cδ is responsible for constitutive and DNA damage-induced phosphorylation of Rad9. EMBO J 2003;22:1431–41.
49. Komatsu K, Miyashita T, Hang H, et al. Human homologue of S. pombe Rad9 interacts with BCL-2/BCL-xL and promotes apoptosis. Nat Cell Biol 2000;2:1–6.
50. Yin Y, Zhu A, Jin YJ, et al. Human RAD9 checkpoint control/proapoptotic protein can activate transcription of p21. Proc Natl Acad Sci U S A 2004;101:8864–9.